PAPER • **OPEN ACCESS**

Modeling resistance increase in a composite ink under cyclic loading

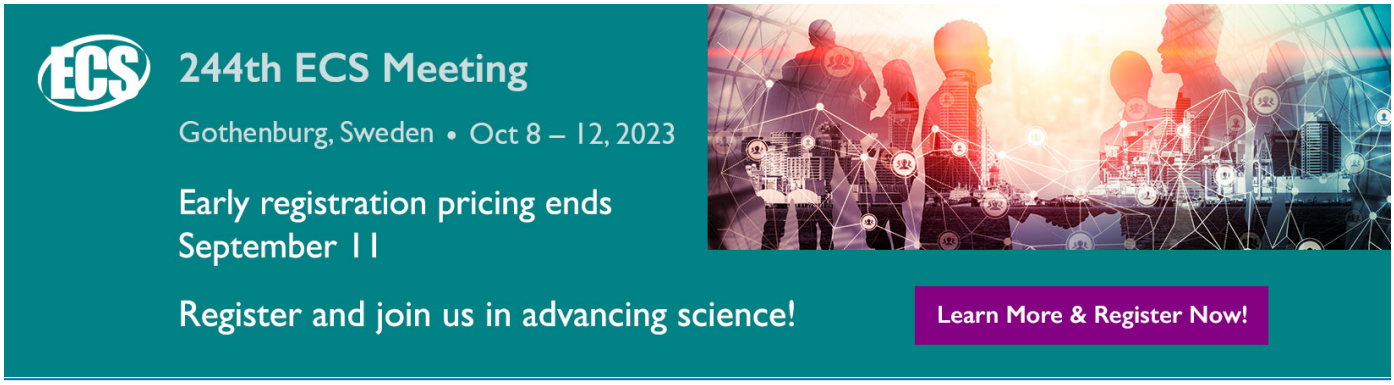

IOP Publishing Flex. Print. Electron. 8 (2023) 015014 https://doi.org/10.1088/2058-8585/acbaab

Flexible and Printed Electronics

PAPER

Modeling resistance increase in a composite ink under cyclic loading

Q Li, E Chung, A Antoniou* and O Pierron*

G.W. Woodruff School of Mechanical Engineering, Georgia Institute of Technology, Atlanta, GA 30318, United States of America
* Authors to whom any correspondence should be addressed.

E-mail: antonia.antoniou@me.gatech.edu and olivier.pierron@me.gatech.edu

Keywords: conductive inks, cyclic stretching, failure lifetime, modeling

Supplementary material for this article is available online

OPEN ACCESS

RECEIVED
23 December 2022

REVISED
3 February 2023

ACCEPTED FOR PUBLICATION
9 February 2023

PUBLISHED
23 February 2023

Abstract

The electrical performance of stretchable electronic inks degrades as they undergo cyclic deformation during use, posing a major challenge to their reliability. The experimental characterization of ink fatigue behavior can be a time-consuming process, and models allowing accurate resistance evolution and life estimates are needed. Here, a model is proposed for determining the electrical resistance evolution during cyclic loading of a screen-printed composite conductive ink. The model relies on two input specimen-characteristic curves, assumes a constant rate of normalized resistance increase for a given strain amplitude, and incorporates the effects of both mean strain and strain amplitude. The model predicts the normalized resistance evolution of a cyclic test with reasonable accuracy. The mean strain effects are secondary compared to strain amplitude, except for large strain amplitudes (>10%) and mean strains (>30%). A trace width effect is found for the fatigue behavior of 1 mm vs 2 mm wide specimens. The input specimen-characteristic curves are trace-width dependent, and the model predicts a decrease in N_f by a factor of up to 2 for the narrower trace width, in agreement with the experimental results. Two different methods are investigated to generate the rate of normalized resistance increase curves: uninterrupted fatigue tests (requiring ∼6–7 cyclic tests), and a single interrupted cyclic test (requiring only one specimen tested at progressively higher strain amplitude values). The results suggest that the initial decrease in normalized resistance rate only occurs for specimens with no prior loading. The minimum-rate curve is therefore recommended for more accurate fatigue estimates.

1. Introduction

Flexible hybrid electronics devices have attracted a lot of research interest in recent years due to their many applications, including wearable healthcare monitoring [1–4], energy storage [5, 6], flexible displays [7–9], and implantable bioelectronics [10, 11]. These devices integrate electronic components with compliant electric circuits based on interconnects that can maintain electrical conductivity under repeated deformation, such as repeated elongation. In wearable device applications, repeated elongation (stretching) of up to 30% strain is typically expected [12]. Various conductive interconnect materials have been studied for their electrical performance under repeated deformation, including thin metal films [13–17], metal nanoparticle inks [18–21], and metal–polymer composite inks [22–28]. One class of metal–polymer composite ink (conductive ink) consists of micron-sized metal flakes embedded in a compliant polymer binder material. The conductive ink is then deposited onto a compliant polymer substrate, typically by screen or gravure printing. The current work used the PE 874 conductive ink provided by DuPont, a stretchable ink with silver flakes embedded in a polyurethane binder and screen-printed on a thermoplastic polyurethane substrate.

As the PE 874 conductive ink is stretched, strain localization occurs in the ink by surface cracking starting from very low strains (∼1%) [28, 29]. In both

the monotonic and cyclic cases, the evolving crack pattern is linked to a resistance increase. From *in-situ* confocal microscope (CM) and scanning electron microscope (SEM) experiments, the surface cracks lengthen as well as deepen and widen with monotonic straining corresponding to a steady increase in electrical resistance up to applied strains of ∼150% [28]. When the ink is cyclically strained between two strain values, the maximum electrical resistance during a cycle also increases with cycling. The *in-situ* CM and SEM cyclic experiments showed that although the extent of the crack pattern does not change with cyclic straining, the cracks that exist at the maximum strain during the first cycle deepen and widen with further cycling [28].

Characterization and modeling of the electrical fatigue behavior of these inks is crucial to design functional stretchable electronics devices with proper reliability. One way to characterize fatigue of a conductive ink specimen is by defining a fatigue life N_f as the number of cycles until a specified normalized resistance R/R_0 (with respect to the initial resistance R_0) is reached, and measuring N_f for different strain amplitudes. Previous work on the PE 874 ink employed critical normalized values of 500 [22] or 100 [28] to define N_f. In each case, a strain amplitude ε_a–fatigue life N_f curve is obtained [22, 28]. The advantage of these curves is that they provide estimates N_f for any given ε_a, using empirical fits relating N_f to ε_a from discrete experimental datasets. However, there are limitations to this approach. First, the ε_a–N_f curve should be obtained for a fixed value of mean strain (ε_m). Even though previous work [28] showed that ε_a has a much more significant effect on N_f than ε_m, the effect of ε_m cannot always for neglected (especially in the case of large ε_m values). Proper characterization would require obtaining several ε_a–N_f curves for different ε_m values. More importantly, the empirical fits obtained from ε_a–N_f curves do not provide any indication of the increase in R/R_0 during cycling. If a different definition of N_f is to be used (say for $R/R_0 = 50$, or 10), a new set of curves needs to be generated. As such, modeling the resistance increase during cycling for any combination of ε_a and ε_m would be much more valuable, which this paper addresses.

Li *et al* [28] showed that the rate of normalized resistance change with cycling, $d(R/R_0)/dN$, or $(R/R_0)'$ for shorthand, is dictated by ε_a. More specifically, $(R/R_0)'$ can be characterized by two values (initial maximum, and minimum values), which were shown to have a strong correlation with ε_a (whereas the effect of ε_m was found to be negligible). The current work presents a model for estimating the R/R_0 evolution during cyclic loading. Figure 1 shows the overall modeling approach in a schematic. The model is based on two input specimen-characteristic curves: either of the $(R/R_0)'$–ε_a curves from cyclic uniaxial test(s) and the R/R_0–ε curve from a monotonic uniaxial test. Importantly, the model accounts for both ε_a and ε_m. From these inputs, the R/R_0 evolution over cycles can be predicted using the model. During each cycle, R/R_0 shifts between a maximum and minimum corresponding to the maximum and minimum strain values respectively, and the maximum R/R_0 measured during a cycle is referred to as R_{max}/R_0 (see examples in figures 2(d) and 3(a)). The predicted R_{max}/R_0 using the model is referred to as $\hat{R}_{max}/R_0$. Modeling the $\hat{R}_{max}/R_0$ evolution over cycles also means that the fatigue life can be predicted—by calculating the number of cycles to reach $\hat{R}_{max}/R_0 = 100$. The predicted fatigue life is referred to as $\hat{N}_f$. Based on the input curves, the ε_a–$\hat{N}_f$ curves can be generated for different values of ε_m. Therefore, the outputs of the model are the $\hat{R}_{max}/R_0$ evolution over cycles and $\hat{N}_f$.

The model is first applied to the 2 mm-wide-specimens fatigue data from Li *et al* [28]. Additional fatigue data are also presented and modeled for a narrower, 1 mm-ink trace width, in order to further assess the effect of trace width on the fatigue behavior [22, 28]. An experimental procedure for obtaining the $(R/R_0)'$–ε_a curve using only one specimen (by performing a series of interrupted cyclic tests at progressively higher ε_a) is also investigated and compared to the procedure where a different specimen is used for each ε_a.

2. Experimental and modeling methods

2.1. Experimental procedures

2.1.1. Fabrication of ink specimens

The PE 874 conductive ink formulated by DuPont is composed of silver flakes embedded in a polyurethane binder material. The average volume fraction of silver flakes, whose sizes range from several μm to 100s of μm, is about 55% [30]. The PE 874 ink test specimens used in this work consist of two layers of the PE 874 ink screen printed onto a thermoplastic polyurethane (TPU) substrate layer in two separate passes. The TPU used for the substrate is the TE-11C from DuPont. The screen-printing process was performed at the DuPont Applications Laboratory with proprietary processes that have been optimized for the ink and substrate. For the first ink layer, a mesh size of 325 threads crossing per inch^2 with wire diameter of 0.9 mil was used. For the second ink layer, a mesh size of 280 threads crossing per inch^2 with wire diameter of 1.2 mil was used. For all cases, the mesh angle was 30°. There was a 15 min drying time after the printing of each ink layer, at 125 °C for the first ink layer and 130 °C for the second layer. The ink is printed in U-shaped, double trace lines with 2 mm or 1 mm trace width (figure 2(a)). The four pads in the print pattern were designed for the four-point electrical resistance probes. The average total thickness of the two ink layers measured by DuPont was 20 μm. The average thickness of the TPU substrate is 127 μm.

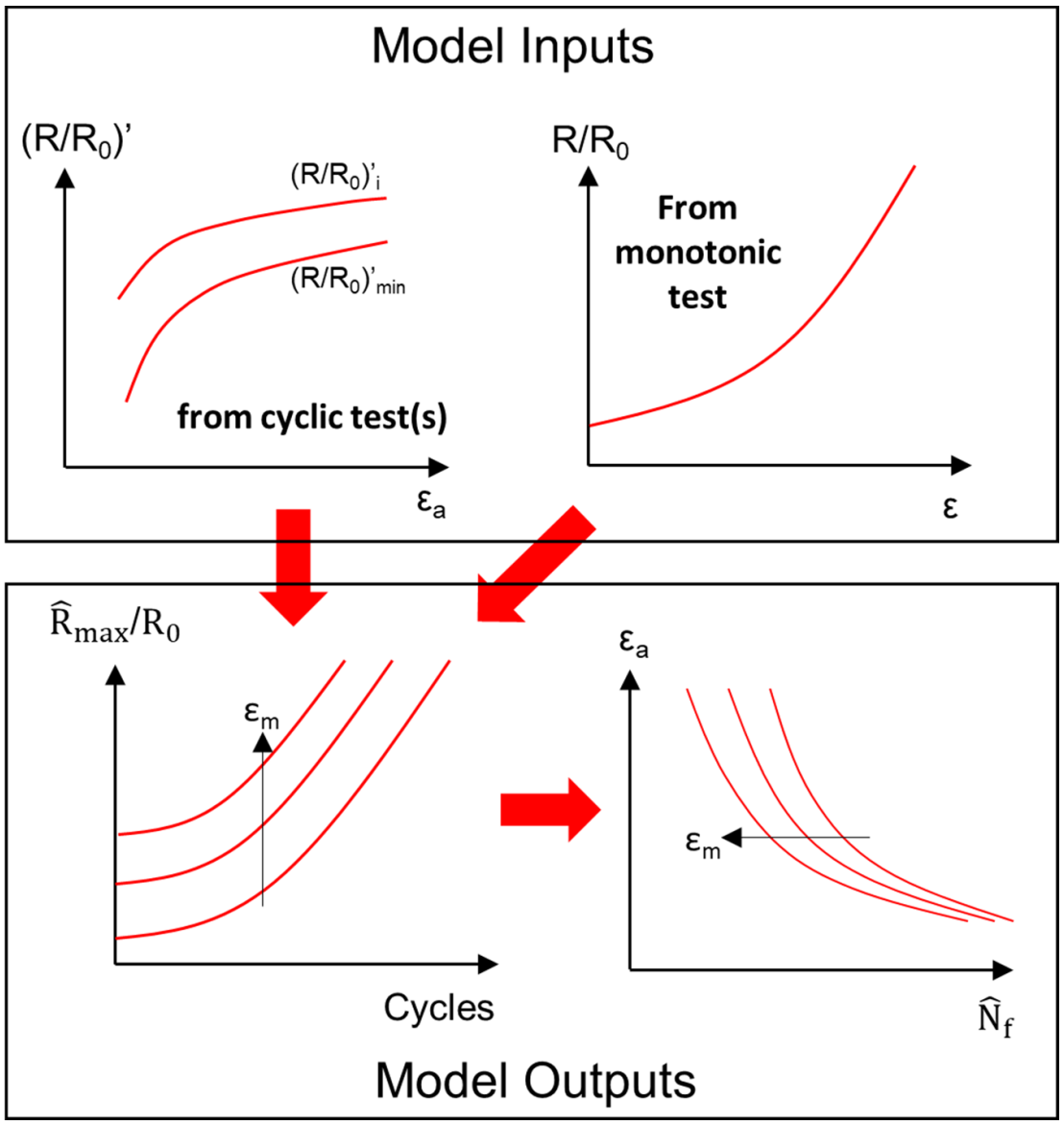

Figure 1. Schematics for overall approach for the model: the rates $(R/R_0)'$–ε_a obtained from a set of cyclic tests and measured R/R_0–ε evolution from a single uniaxial monotonic test are the input; the predicted $\hat{R}_{max}/R_0$ evolution over cycles and predicted fatigue life $\hat{N}_f$ are the output.

2.1.2. Cyclic test procedures

The cyclic uniaxial stretching tests were performed with synchronous electrical resistance measurements on the Linkam Scientific TST350 Microtensile Test Stage (figure 2(b)) at a strain rate of 2% per second. The electrical resistance is measured using the Agilent 34401A digital multimeter. The cyclic stretching tests were performed by first stretching the test specimen to the maximum strain $\varepsilon_m + \varepsilon_a$ (mean strain plus strain amplitude), and then cycling between the maximum strain $\varepsilon_m + \varepsilon_a$ and minimum strain $\varepsilon_m - \varepsilon_a$. In addition, a series of interrupted cyclic tests were performed, in order to obtain relevant rate parameters for a range of ε_a's using only one specimen. For the interrupted tests firstly, a cyclic test was performed at a low ε_a (2% in the current work) for ten cycles, then the test specimen was unloaded. Next another test was performed at a higher ε_a on the same specimen for only ten cycles, then the specimen was again unloaded. This process is repeated for progressively higher ε_a up to 18%. Figures 2(c)–(f) show schematics of the strain and R/R_0 evolution over cycles for an uninterrupted (figures 2(c)–(d)) versus interrupted (figures 2(e)–(f)) test. A table of the sets of cycles used for the interrupted test is shown in figure 2(g).

The resistance is reported as the normalized value R/R_0, where R is the current resistance and R_0 is the initial resistance before testing. Due to the distance d_{clamp} between the specimen clamps (about 30 mm) being shorter than half the overall length l_{print} of the double trace line (38 mm), the initial resistance R_0 needed to be adjusted for the unstrained portion of the specimen:

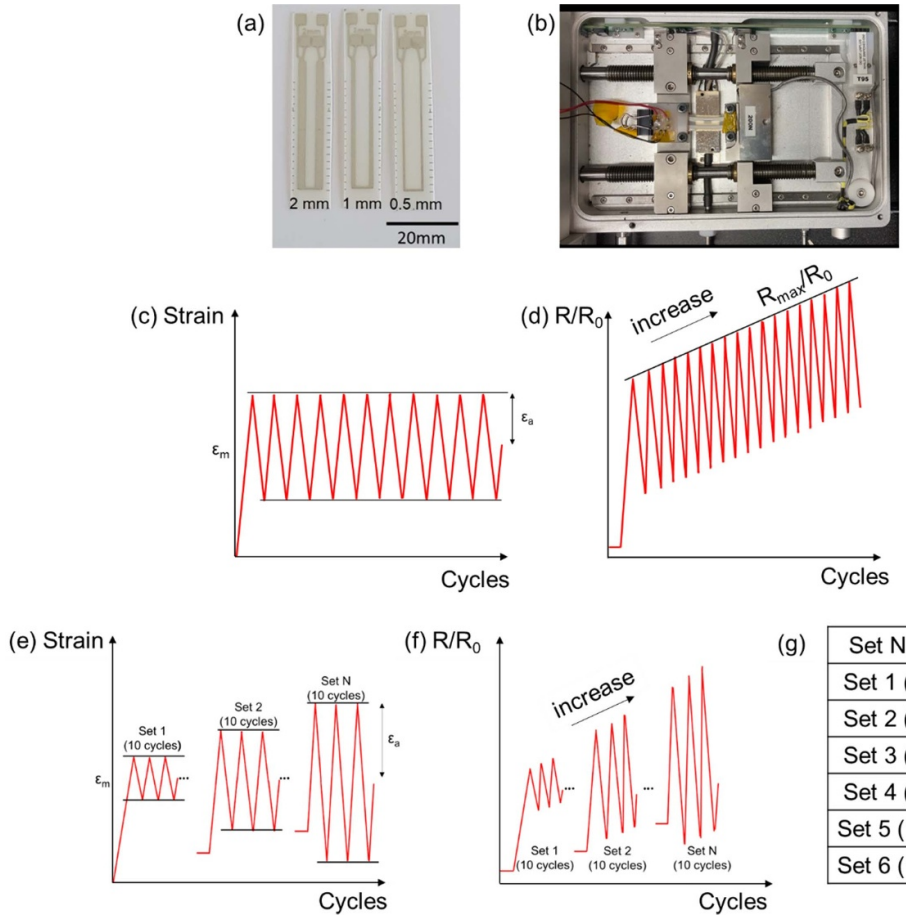

(g)

Set N (ε_a)	N (cycles)
Set 1 (2%)	1~10
Set 2 (4%)	11~20
Set 3 (6%)	21~30
Set 4 (8%)	31~40
Set 5 (12%)	41~50
Set 6 (15%)	51~60

Figure 2. (a) PE874 ink test specimens with different trace widths; (b) experimental setup using the Linkam TST350 test stage; schematics of (c) strain-cycles and (d) R/R_0-cycles for an uninterrupted cyclic test, and of (e) strain-cycles and (f) R/R_0-cycles for the interrupted cyclic test; (g) table of sets of cycles at different ε_a for the interrupted cyclic test.

$$R_0 = R_{\text{full specimen, }\varepsilon=0} \times \left(\frac{d_{\text{clamp}}}{l_{\text{print}}/2}\right) \quad (1)$$

The resistance R is the sum of the initial resistance R_0 and the measured change in resistance ΔR, which is entirely attributed to the strained portion of the specimen:

$$\Delta R = R_{\text{full specimen},\varepsilon} - R_{\text{full specimen},\varepsilon=0} \quad (2)$$

$$R = R_0 + \Delta R. \quad (3)$$

2.1.3. Determination of rate of normalized resistance increase

The rate of resistance change with cycling, $(R/R_0)'$, at any cycle N was calculated by fitting a linear regression function to the measured R_{max}/R_0 evolution over cycling (see examples in figures 3(a)–(d)) between $N-4$ and $N+4$, excluding any null points at the beginning or end of the set of cycles. The choice of using the cycles $N-4$ to $N+4$ for the linear regression fitting was made by trial to achieve the generally smooth evolution of $(R/R_0)'$ over the cycles. The initial rate $(R/R_0)'_i$ and minimum rate $(R/R_0)'_{\text{min}}$ were identified in [28] as relevant rate parameters for characterizing resistance evolution with cycling.

The evolution of $(R/R_0)'$ with cycling for 2 mm-wide-specimens is summarized in figure 3. For $\varepsilon_a \geqslant 3\%$, the normalized resistance always increases with cycling ($(R/R_0)' > 0$); moreover, $(R/R_0)'$ initially decreases with cycling until reaching a minimum value, after which $(R/R_0)'$ increases significantly (see figure 3(e)). In that large $(R/R_0)'$ stage (where R/R_0 increases by more than 5 times every cycle), the ink is not considered functional anymore. For $\varepsilon_a = 1$ or 2%, the normalized resistance tends to first decrease within the few cycles ($(R/R_0)' < 0$), after which it slowly increases (see figure 3(f)). The initial decrease in R/R_0 is likely associated with relaxation of the substrate (as shown in [22] when holding a specimen at constant strain), and the fact that the fatigue damage is not significant enough to result in a large R/R_0 increase to counteract the small relaxation effects. As a result, the $(R/R_0)'$ is maximum at cycle ~10–50, then decreases with cycling until reaching a steady-state minimum value. The initial rate $(R/R_0)'_i$ is defined by the initial local maximum in the $(R/R_0)'$ evolution. For $\varepsilon_a \geqslant 3\%$, $(R/R_0)'_i$ was found to occur at cycle 1; for $\varepsilon_a = 1\%$ or 2%, $(R/R_0)'_i$ occurs at a later cycle but within the first 50 cycles for the aforementioned reason (see figure 3(f)). The minimum rate $(R/R_0)'_{\text{min}}$

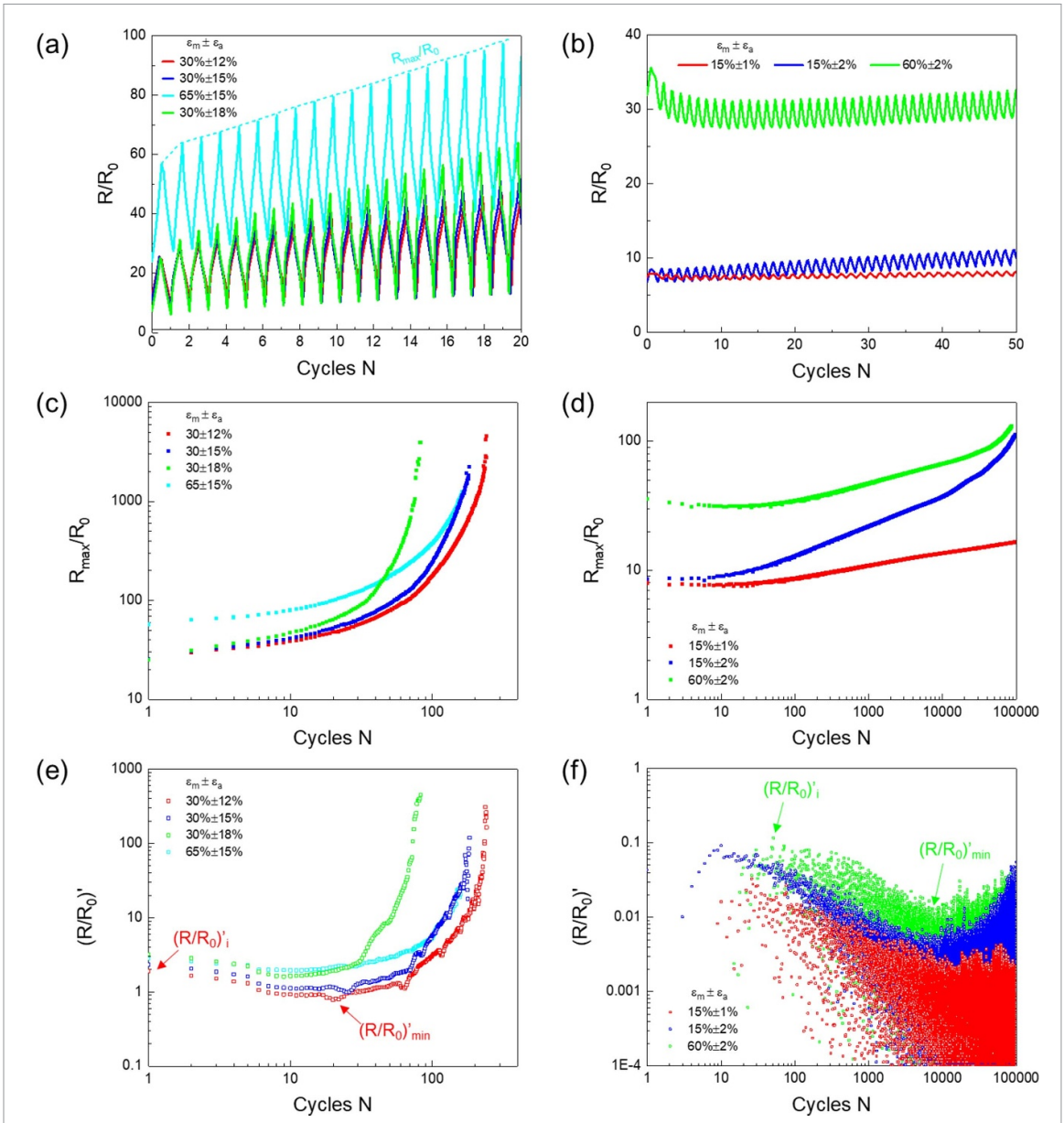

Figure 3. R/R_0 evolution over the initial cycles for (a) selected high ε_a tests with the envelope of R_{max}/R_0 marked for the 65 ± 15% ($\varepsilon_m \pm \varepsilon_a$) test, and (b) selected low ε_a tests; R_{max}/R_0 evolution for (c) selected high ε_a tests, and (d) selected low ε_a tests; $(R/R_0)'$ evolution over cycles for (e) selected high ε_a tests with the $(R/R_0)'_i$ and $(R/R_0)'_{min}$ marked for the 30 ± 12% test, and (f) selected low ε_a tests with the $(R/R_0)'_i$ and $(R/R_0)'_{min}$ marked for the 60 ± 2% test. All tests used 2 mm trace width specimens.

is defined by the absolute minimum $(R/R_0)'$ for cases with $\varepsilon_a \geqslant 10\%$ or the minimum of the upper bound of the $(R/R_0)'$ data for cases with $\varepsilon_a < 10\%$, given the large spread in the $(R/R_0)'$ data for these cases (see figure 3(f)). $(R/R_0)'_{min}$ occurred at 10's of cycles for the high ε_a tests and 1000's of cycles for the low ε_a tests. An alternative method for obtaining the rate parameters was implemented with the interrupted test described in section 2.1.2. For that method, the minimum $(R/R_0)'$ during a set of ten cycles (at a given ε_a) was used as the $(R/R_0)'_{min}$ parameter for that ε_a.

2.2. Model of normalized resistance evolution under cyclic loading

A simple model is derived to predict resistance increase as a function of the number of applied cycles N. For the first cycle ($N = 1$), $\hat{R}_{max}/R_0$ is obtained at the maximum strain value $\varepsilon_m + \varepsilon_a$ during the cycle, which can be obtained from the monotonic data. The additional increase in $\hat{R}_{max}/R_0$ with cycling is assumed to be linear with the number of cycles (constant $(R/R_0)'$). Using the maximum initial rate $(R/R_0)'_i$ provides a conservative model, as follows:

$$\frac{\hat{R}_{max}}{R_0} = \left(\frac{R_{max}}{R_0}\right)_{N=1} + (N-1)\left(\frac{R}{R_0}\right)'_i. \quad (4)$$

A fatigue live $\hat{N}_f$ can also be predicted. If failure is determined by $\hat{R}_{max}/R_0 = 100$, $\hat{N}_f$ is:

$$\hat{N}_f = \frac{100 - \left(\frac{R_{max}}{R_0}\right)_{N=1}}{\left(\frac{R}{R_0}\right)'_i} + 1\,. \quad (5)$$

The $\hat{R}_{max}/R_0$ of the first cycle as a function of ε_m and ε_a is obtained from the polynomial fit of the R/R_0–ε data from a single monotonic test. The $(R/R_0)'_i$ as a function of ε_a is obtained from the power law function fit of the $(R/R_0)'_i$–ε_a data from a set of cyclic tests. The model for $\hat{R}_{max}/R_0$ and $\hat{N}_f$ can be similarly formulated using $(R/R_0)'_{min}$:

$$\frac{\hat{R}_{max}}{R_0} = \left(\frac{R_{max}}{R_0}\right)_{N=1} + (N-1)\left(\frac{R}{R_0}\right)'_{min} \quad (6)$$

$$\hat{N}_f = \frac{100 - \left(\frac{R_{max}}{R_0}\right)_{N=1}}{\left(\frac{R}{R_0}\right)'_{min}} + 1. \quad (7)$$

Although the current model focuses on $\hat{R}_{max}/R_0$ during the cycle at the maximum strain, analogous models can be derived for strain values during the cycle other than the maximum strain. For any strain value during the cycle, $(R/R_0)_{N=1}$ can be obtained at the strain value from a monotonic test and $(R/R_0)'_i$ and $(R/R_0)'_{min}$ at the strain value can be obtained from cyclic tests in an analogous manner to those defined for R_{max}/R_0.

3. Results and discussion

3.1. Modeling results for 2 mm-wide specimens: R/R_0 evolution and N_f estimates

Figure 4 shows the measured data for the 2 mm-wide specimens (obtained from [28]) that are fitted to serve as input for our model: R/R_0–ε evolution from a monotonic test (figure 4(a)) and $(R/R_0)'_i$ and $(R/R_0)'_{min}$ versus ε_a from cyclic tests (figure 4(b)). The correlation between the rate parameters and ε_a are reasonably fitted by a power law function, even though different ε_m values were used in the 2 mm-wide tests. Figure 5(a) shows the $\hat{R}_{max}/R_0$ evolution (in a semi-log format) predicted by the model, using both minimum and initial maximum $(R/R_0)'$ values, along with the measured R_{max}/R_0 evolution for selected 2 mm-wide specimens. As expected, $(R/R_0)'_i$ provides a more conservative $\hat{R}_{max}/R_0$ evolution over the cycles than $(R/R_0)'_{min}$. The difference between both modeled curves is more significant for lower ε_a values (see for example the $\hat{R}_{max}/R_0$ curves for $\varepsilon_a = 2\%$ vs 18%), given the larger differences between $(R/R_0)'_i$ and $(R/R_0)'_{min}$ in the low ε_a regime (see figure 4(b)). Overall, the $\hat{R}_{max}/R_0$ curves using $(R/R_0)'_{min}$ are closer to the measured R_{max}/R_0 evolution than that using $(R/R_0)'_i$. These curves are more accurate for the larger ε_a values (>5%). For $\varepsilon_a = 2\%$, the model is reasonably accurate for the first 1000 cycles, after which the model departs significantly from the measured R_{max}/R_0 evolution. The inaccuracy for $\varepsilon_a = 2\%$ is due to the overestimation of $(R/R_0)'_{min}$, given the large spread of $(R/R_0)'$ measured after 1000 cycles with these low ε_a tests (see figure 3(f)).

Figure 5(b) compares the modeled ε_a–$\hat{N}_f$ curves for three different ε_m values, using both $(R/R_0)'_i$ and $(R/R_0)'_{min}$, to the measured N_f for 2 mm-wide specimens (obtained from [28]). The modeled curves are nearly identical for $\varepsilon_m = 15\%$ and 30%, capturing the fact that ε_m has a secondary effect on N_f. The effect of ε_m is non-negligible only for large ε_m (60%) and ε_a values (>10%) values, as also highlighted by the two fatigue tests at $\varepsilon_a = 15\%$ ($N_f = 55$ cycles for $\varepsilon_m = 30\%$, and 22 cycles for $\varepsilon_m = 65\%$). Overall, the modeled ε_a–$\hat{N}_f$ curves using $(R/R_0)'_{min}$ are consistently closer to the measured N_f than those using $(R/R_0)'_i$, which are more conservative (especially for $\varepsilon_a \leqslant 3\%$).

3.2. Effect of trace width (1 vs 2 mm) on fatigue properties and model

The trace width effect on the electrical behavior of the PE 874 ink has been investigated previously, mainly for monotonic loading [29]. The size effect was related to the crack size being commensurate with the trace widths, the same crack pattern having a more detrimental effect on resistance for smaller trace widths. As such, size effects are not expected for trace widths larger than 2 mm, and the input curves shown in figure 4 could be used to model the fatigue behavior of wide traces. However, the relationship between trace width and fatigue behavior requires additional characterization for narrower traces. Figure 6 shows the R/R_0–ε evolution curve and the $(R/R_0)'_i$ and $(R/R_0)'_{min}$ vs ε_a curves for 1 mm-wide specimens, along with the respective curves for 2 mm-wide specimens. All 1 mm-wide specimens were tested with the same $\varepsilon_m = 30\%$ (the 2 mm-wide data are from [28], where a range of ε_m was used). These figures highlight the extent of trace width effect on the input parameters for our resistance evolution model: the initial resistance (at cycle 1) at the maximum applied strain is increased by up to ~50%–60% for the 1 mm-wide specimens (see figure 6(a)), and the rates $(R/R_0)'$ are increased by a factor of up to 2, especially for larger ε_a values (see figure 6(b)). For example, for $\varepsilon_a = 18\%$ and $\varepsilon_m = 30\%$, $(R/R_0)_i'$ is 3.22 for 2 mm and 6.11 for 1 mm. The input curves are therefore not solely ink-specific but instead ink- and geometry-specific. This is because the resistance evolution is related to crack evolution [28], and the effect of cracking on resistance is dependent on trace width. The 2 mm data can be used for wider traces, but not but narrower traces.

The trace width effect on the measured R_{max}/R_0 evolution and the models is illustrated in figure 7(a) for a fatigue test at $\varepsilon_m = 30\%$ and $\varepsilon_a = 15\%$. The experimental curves highlight that the main effect is related to the initial R/R_0 value (for cycle 1), which is twice larger for 1 mm (see figure 6(a)). The figure also shows that the models are much more accurate when using the input data from the correct specimen width. The same conclusion applies for the ε_a–N_f

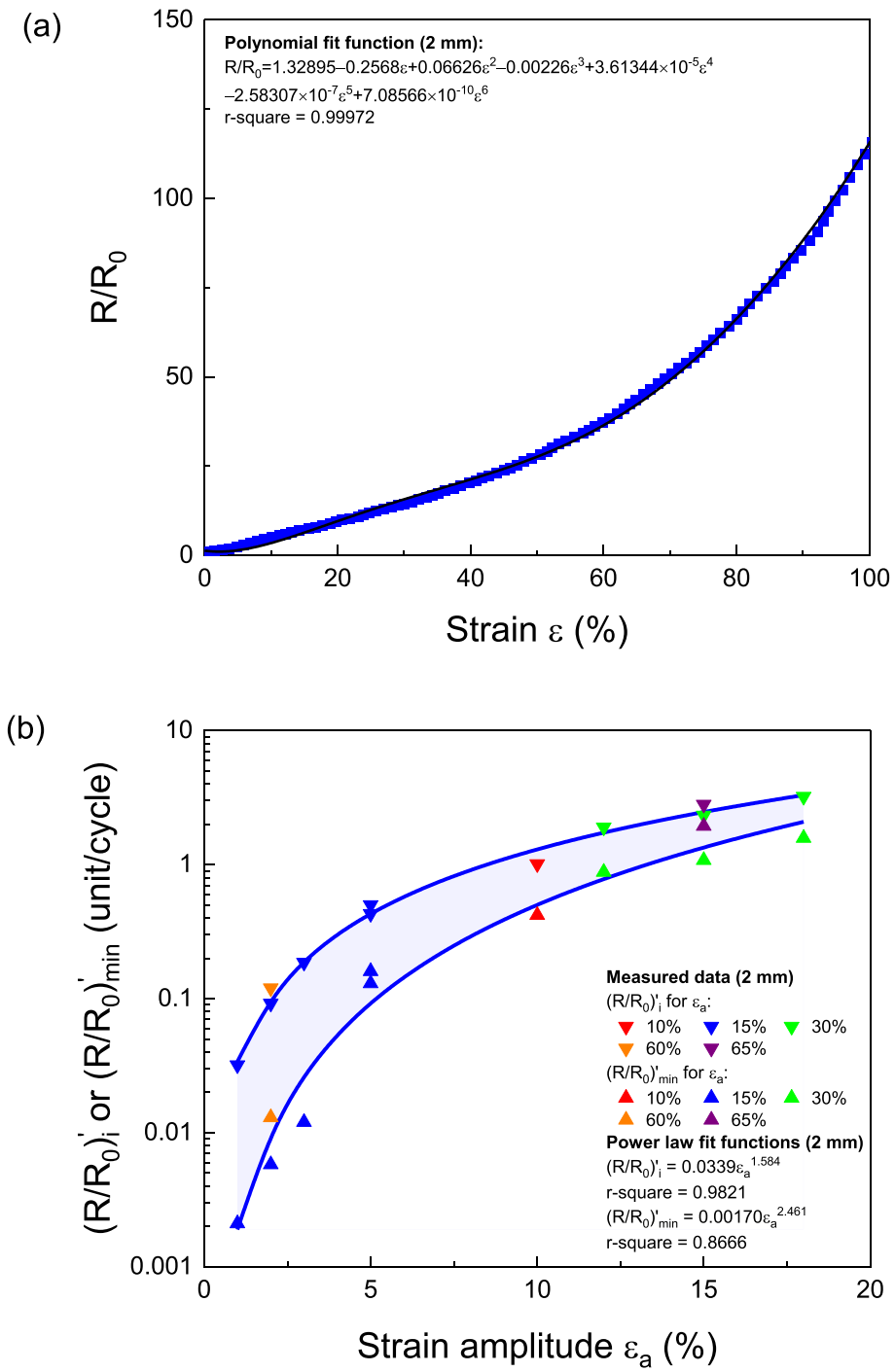

Figure 4. Input specimen-characteristic curves for the model. (a) Polynomial fit of experimental data of R/R_0–ε for 2 mm-wide-specimens (monotonic test); (b) $(R/R_0)'_i$ and $(R/R_0)'_{min}$ for 2 mm-wide specimens as a function of ε_a. The solid lines show the power law fit.

curves; see figure 7(b) ($\varepsilon_m = 30\%$ for the 1 mm data; for the 2 mm data, only ε_m in the 15%–30% range is shown, as the effects are negligible in that range). The measured N_f is consistently lower for the 1 mm-wide specimens, which is why the modeling is trace width-dependent (for trace widths less than 2 mm). The modeled $\hat{N}_f$ is about twice lower at $\varepsilon_a = 15\%$ for 1 mm.

3.3. Determining normalized resistance increase rates using interrupted cyclic tests

The $(R/R_0)'$–ε_a curves shown in figures 4(b) and 6(b) were obtained by using as many specimens as data-points (1 datapoint per specimen); see examples in figure 3. The rate curves obtained for 1 mm-wide specimens (see figure 6(b)) are compared to curves obtained from an interrupted cyclic test (see

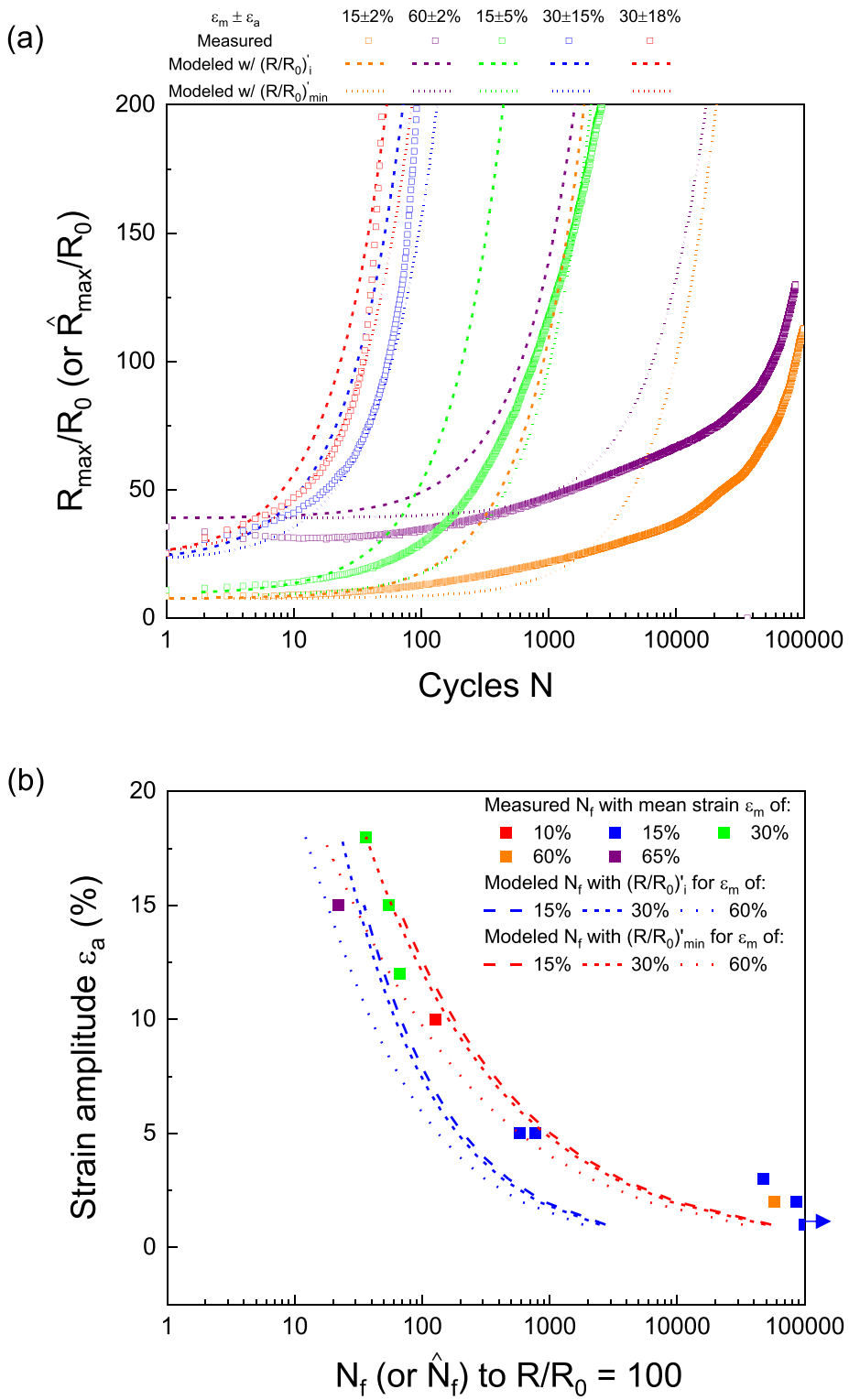

Figure 5. (a) R_{max}/R_0 and $\hat{R}_{max}/R_0$ evolution over cycles N, measured and modeled using $(R/R_0)'_i$ and $(R/R_0)'_{min}$, for selected 2 mm-wide specimens; (b) strain amplitude ε_a versus measured (N_f) and modeled ($\hat{N}_f$) fatigue life using $(R/R_0)'_i$ and $(R/R_0)'_{min}$, for 2 mm-wide specimens.

figures 2(e), (f) and section 2.1.2), in order to assess whether the required input data for the model can be obtained with as few experiments as possible. The results of an interrupted cyclic test are shown in figure S1 of the supporting information. For most ε_a (2%, 4%, 12%, and 15%), there is a decrease in R_{max}/R_0 between the first and second cycle, after which R_{max}/R_0 increases with cycling. This initial value is not included in the calculations, as it is likely related to polymer substrate relaxation due to the unloading/reloading between each ε_a used for this method. Figure 8 compares the $(R/R_0)'$ evolution over cycles from the uninterrupted tests (figure 8(a)) and the interrupted test (figure 8(b), starting at $N = 2$).

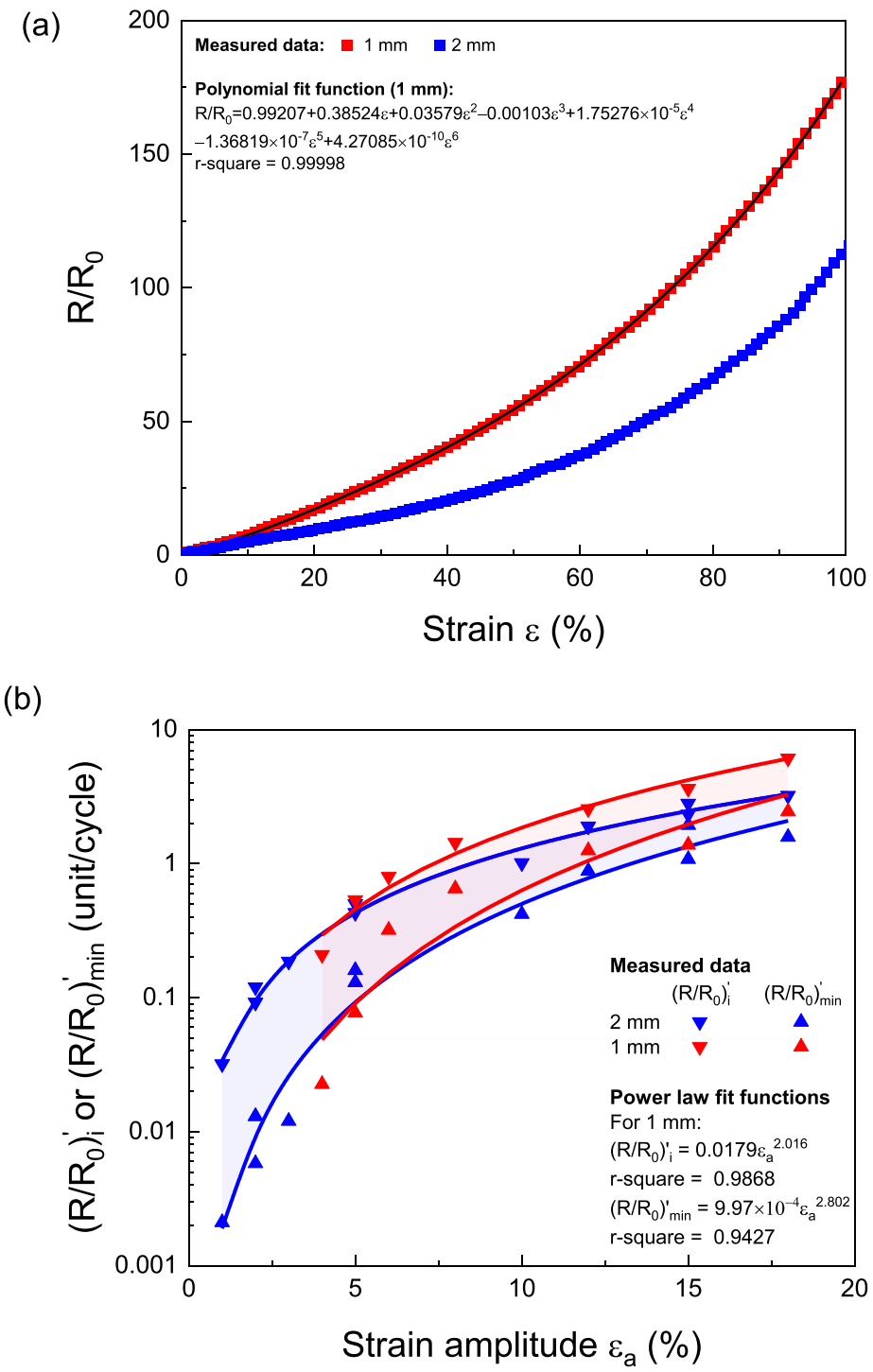

Figure 6. (a) R/R_0–ε for 1 mm and 2 mm-wide specimens (monotonic tests) and polynomial fit; (b) $(R/R_0)'_i$ and $(R/R_0)'_{min}$ for 1 mm and 2 mm-wide specimens with different ε_a and power law fit functions.

The main difference between the two methods is the absence of initial decrease in rates for the interrupted test. As summarized in section 2.1.3, for the uninterrupted tests, $(R/R_0)'$ initially decreases with cycling for all ε_a values (for $\varepsilon_a = 1\%$ or 2%, there is initially a decrease in R_{max}/R_0 within the first 30 cycles, before a local maximum initial value in $(R/R_0)'$ is reached). This difference highlights that the initial decrease in $(R/R_0)'$ is not an intrinsic property of the specimen, but instead an artifact associated with testing an ink with no prior loading history. Additional interrupted tests (not shown here) did have an initial decrease in $(R/R_0)'$ for the first ε_a value (say, $\varepsilon_a = 4\%$), but not for the following ε_a values, indicating that the initial decrease in $(R/R_0)'$ only occurs if the ink had no prior loading. The reason for this behavior is unclear. One possibility is the presence of residual tensile stress in the ink. From a practical viewpoint, the model using $(R/R_0)'_i$ values should not be used to estimate the fatigue behavior of an ink with prior loading history.

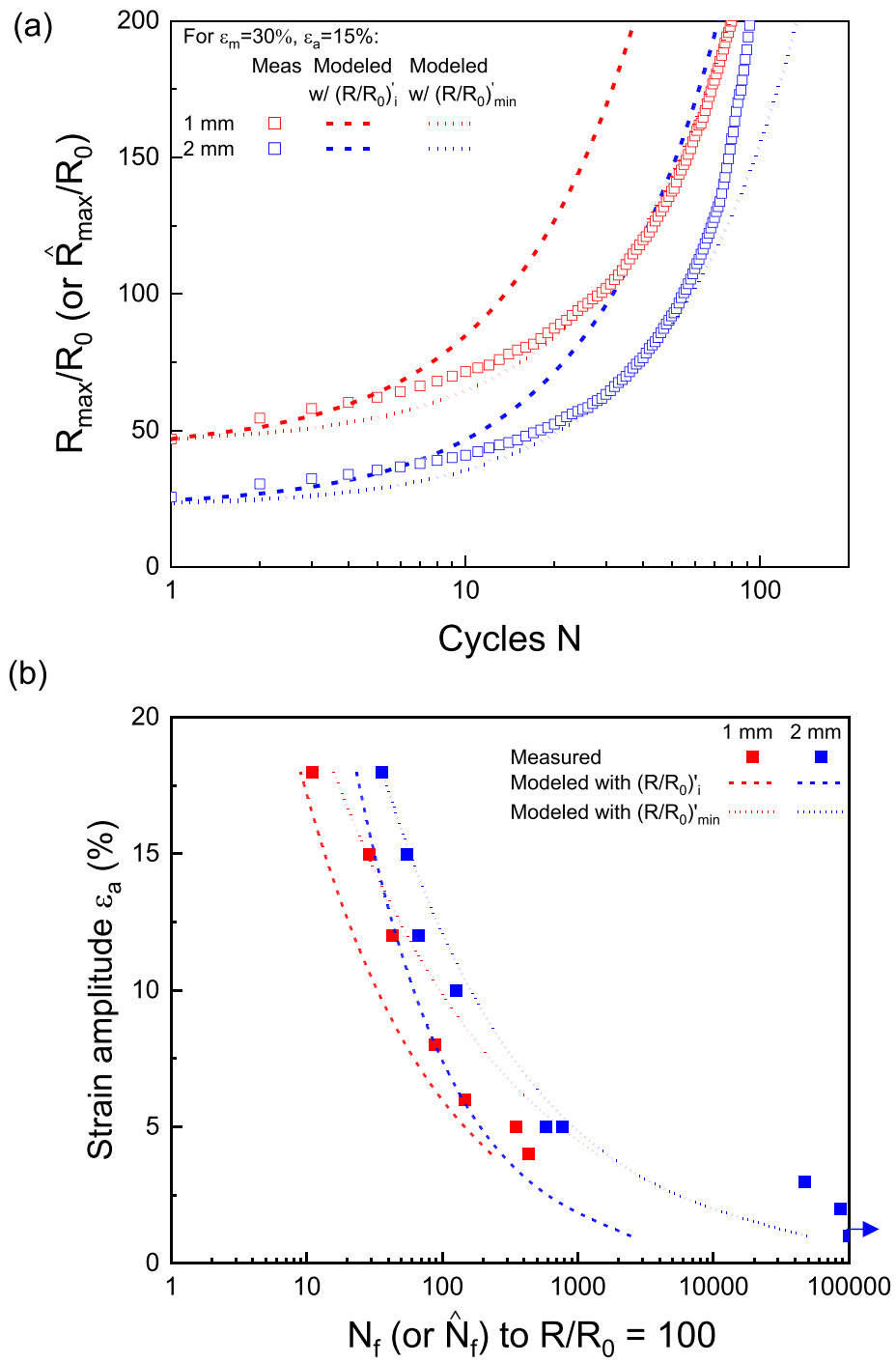

Figure 7. (a) R_{max}/R_0 and $\hat{R}_{max}/R_0$ evolution over cycles, measured and modeled using $(R/R_0)'_i$ and $(R/R_0)'_{min}$, for 1 mm and 2 mm-wide specimens, for a fatigue test at $\varepsilon_a = 15\%$ and $\varepsilon_m = 30\%$; (b) strain amplitude ε_a versus measured (N_f) and modeled ($\hat{N}_f$) fatigue life using $(R/R_0)'_i$ and $(R/R_0)'_{min}$, for 1 mm ($\varepsilon_m = 30\%$) and 2 mm-wide specimens.

Figure 9(a) compares the $(R/R_0)'_{min}$ obtained from the interrupted test and the uninterrupted tests. The $(R/R_0)'_{min}$ from the interrupted test are in close agreement with the $(R/R_0)'_{min}$ obtained from the uninterrupted tests. A power law function was also used to fit the $(R/R_0)'_{min}$–ε_a data for the interrupted test. The fact that the two fitting functions for $(R/R_0)'_{min}$–ε_a, obtained from interrupted and uninterrupted tests, are similar is remarkable. It implies that reasonable fatigue estimates can be obtained using the interrupted test, which requires only one specimen (as opposed to seven specimens for the uninterrupted tests). It also implies that the minimum rate is not affected by prior loading history. Li *et al* demonstrated that the normalized resistance increase during fatigue is related to simultaneous widening and deepening of cracks. Therefore, it is likely that prior loading does not affect the way crack widening and deepening occurs at a given ε_a, and it effects on (R/R_0). Figure 9(b) compares the

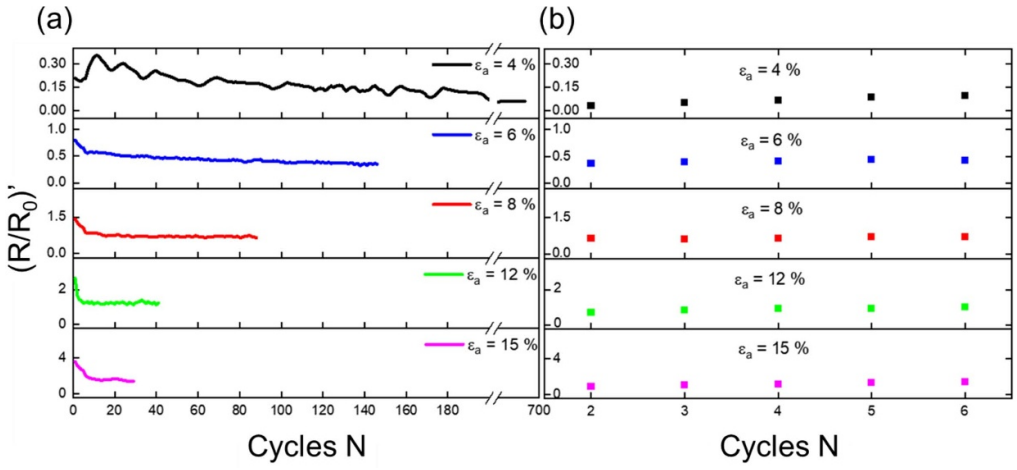

Figure 8. $(R/R_0)'$ evolution over cycles for (a) uninterrupted tests and (b) interrupted test with 1 mm-wide specimens at ε_m of 30% and different ε_a (4%, 6%, 8%, 12%, 15%).

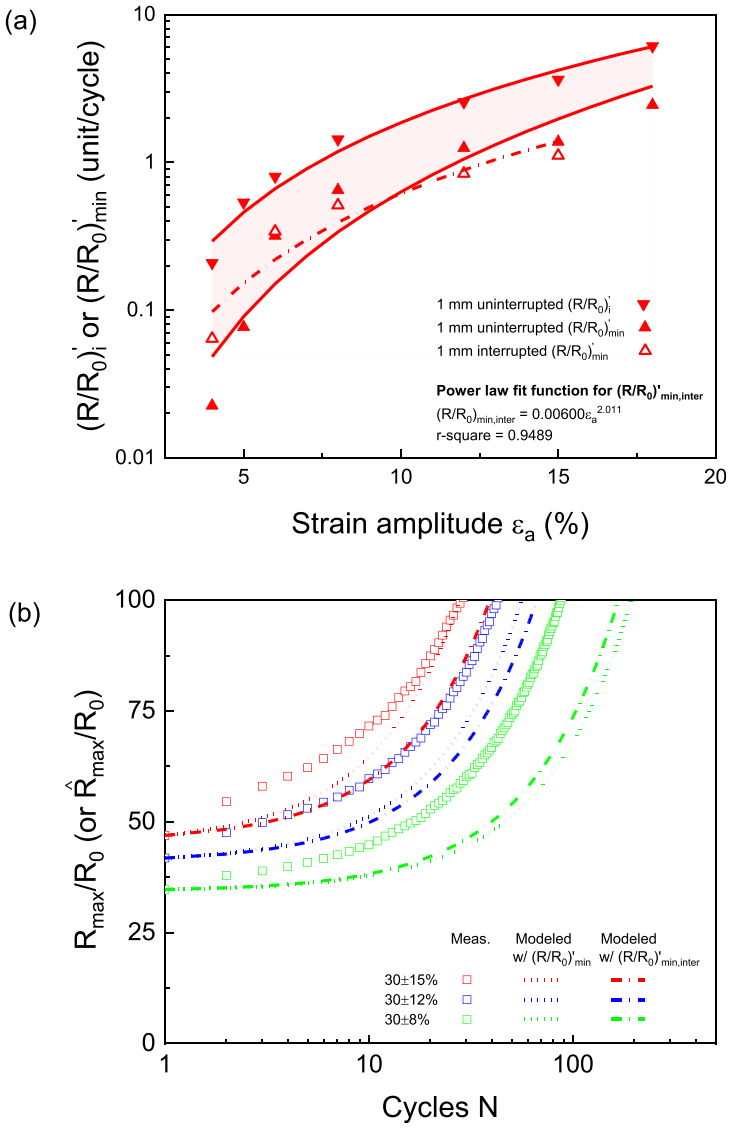

Figure 9. (a) $(R/R_0)'$ parameters for 1 mm-wide specimens using interrupted and uninterrupted tests with different strain amplitudes ε_a and power law fit functions for $(R/R_0)'_i$–ε_a and $(R/R_0)'_{min}$–ε_a. (b) R_{max}/R_0 and $\hat{R}_{max}/R_0$ evolution over cycles N, measured and modeled using interrupted and uninterrupted curves, for two 1 mm-wide specimens.

modeled $\hat{R}_{max}/R_0$ evolution based on the interrupted test fitting function, with the measured R_{max}/R_0 for three fatigue tests (ε_m = 30%, ε_a = 8%, 12%, and 15%). The figure also shows the models based on $(R/R_0)'_{min}$ from the uninterrupted tests. Both models provide very similar $\hat{R}_{max}/R_0$ evolution, and are in good agreement with the experimental data.

4. Conclusions

The following is a summary of results regarding the formulation and implementation of a rate-based model for predicting electrical resistance evolution and fatigue life of the conductive ink PE 874 under cyclic strain.

- A model to estimate R/R_0 evolution with cycling as well as fatigue life N_f (as defined by the number of cycles to reach a threshold value of R/R_0, such as 100) was constructed by using two input specimen-characteristic curves: R/R_0 vs ε from a monotonic stretch test, and either $(R/R_0)'_i$–ε_a or $(R/R_0)'_{min}$–ε_a from a set of cyclic stretch tests. The model assumes a constant rate of normalized resistance increase, and incorporates the effects of both ε_m and ε_a.
- The model predicts the R_{max}/R_0 evolution for a cyclic stretch test with strain amplitude ε_a and mean strain ε_m with reasonable accuracy, especially when using the $(R/R_0)'_{min}$–ε_a input curve. The $(R/R_0)'_i$–ε_a curve provides a more conservative estimate but is inaccurate at low ε_a (<5%). The mean strain effects are mainly secondary compared to strain amplitude, except for large ε_a (>10%) and large ε_m (>30%).
- A trace width effect is found for the fatigue behavior of 1 mm vs 2 mm-wide specimens. The input specimen-characteristic curves are trace-width dependent, and the model predicts a decrease in N_f by a factor of up to 2 for the narrower trace width, in agreement with the experimental results.
- Two different methods were investigated to generate the $(R/R_0)'$–ε_a curves: uninterrupted fatigue tests (requiring ~6–7 cyclic tests to generate the curve), and a single interrupted cyclic test (requiring only 1 specimen tested at progressively higher ε_a to generate the curve). The interrupted test can reproduce the $(R/R_0)'_{min}$–ε_a curve obtained from the uninterrupted tests with reasonable agreement. However, it cannot reproduce the initial maximum rates $(R/R_0)'_i$, since it does not exhibit an initial decrease in rates. The results suggest that the initial decrease in rate only occurs for specimen with no prior loading. The minimum-rate curve is therefore recommended for more accurate fatigue estimates.

Although the current model is specifically for the PE874 ink, it is likely to be applicable for other inks that exhibit a similar fatigue behavior related to ink fatigue cracking.

Data availability statement

The data cannot be made publicly available upon publication due to legal restrictions preventing unrestricted public distribution. The data that support the findings of this study are available upon reasonable request from the authors.

Acknowledgments

The authors gratefully acknowledge funding support from the National Science Foundation (NSF CMMI-MOMS: 2026936). The authors are grateful to DuPont colleagues (Jeff Meth, Lynne Dellis and Augustus Jones) for providing samples.

ORCID iDs

Q Li https://orcid.org/0000-0003-3574-8230
E Chung https://orcid.org/0000-0001-7602-5069
A Antoniou https://orcid.org/0000-0002-5270-5438
O Pierron https://orcid.org/0000-0003-0787-7457

References

[1] Gao W *et al* 2016 Fully integrated wearable sensor arrays for multiplexed *in situ* perspiration analysis *Nature* **529** 509–14
[2] Imani S, Bandodkar A J, Mohan A M V, Kumar R, Yu S, Wang J and Mercier P P 2016 A wearable chemical–electrophysiological hybrid biosensing system for real-time health and fitness monitoring *Nat. Commun.* **7** 1–7
[3] Lee H *et al* 2016 A graphene-based electrochemical device with thermoresponsive microneedles for diabetes monitoring and therapy *Nat. Nanotechnol.* **11** 566–72
[4] Stewart B G, Cahn G, Samet D, Misner M J, Burns A, Weerawarne D L, Poliks M D, Lapinski C, Dugan S and Pierron O 2020 Mechanical deformation study of flexible leadset components for electromechanical reliability of wearable electrocardiogram sensors *2020 IEEE 70th Electronic Components and Technology Conf. (ECTC)* (IEEE) pp 532–40
[5] Dubal D P, Chodankar N R, Kim D-H and Gomez-Romero P 2018 Towards flexible solid-state supercapacitors for smart and wearable electronics *Chem. Soc. Rev.* **47** 2065–129
[6] Lv T, Liu M, Zhu D, Gan L and Chen T 2018 Nanocarbon-based materials for flexible all-solid-state supercapacitors *Adv. Mater.* **30** 1–17
[7] Kim S *et al* 2011 Low-power flexible organic light-emitting diode display device *Adv. Mater.* **23** 3511–6
[8] Rogers J A *et al* 2001 Paper-like electronic displays: large-area rubber-stamped plastic sheets of electronics and microencapsulated electrophoretic inks *Proc. Natl Acad. Sci.* **98** 4835–40
[9] Sekitani T, Nakajima H, Maeda H, Fukushima T, Aida T, Hata K and Someya T 2009 Stretchable active-matrix organic light-emitting diode display using printable elastic conductors *Nat. Mater.* **8** 494–9
[10] Hong Y J, Jeong H, Cho K W, Lu N and Kim D H 2019 Wearable and implantable devices for cardiovascular healthcare: from monitoring to therapy based on flexible and stretchable electronics *Adv. Funct. Mater.* **29** 1–26

[11] KIm D *et al* 2011 Materials for multifunctional balloon catheters with capabilities in cardiac electrophysiological mapping and ablation therapy *Nat. Mater.* **10** 316–23
[12] Chow J H, Sitaraman S K, May C and May J 2018 Study of wearables with embedded electronics through experiments and simulations *2018 IEEE 68th Electronic Components and Technology Conf. (ECTC)* (IEEE) pp 814–21
[13] Gebhart D D, Krapf A, Gammer C, Merle B and Cordill M J 2022 Linking through-thickness cracks in metallic thin films to *in-situ* electrical resistance peak broadening *Scr. Mater.* **212** 114550
[14] Glushko O, Klug A, List-Kratochvil E and Cordill M 2016 Relationship between mechanical damage and electrical degradation in polymer-supported metal films subjected to cyclic loading *Mater. Sci. Eng.* A **662** 157–61
[15] Graz I M, Cotton D P J and Lacour S P 2009 Extended cyclic uniaxial loading of stretchable gold thin-films on elastomeric substrates *Appl. Phys. Lett.* **94** 071902
[16] Sim G-D, Hwangbo Y, Kim H H, Lee S-B and Vlassak J J 2012 Fatigue of polymer-supported Ag thin films *Scr. Mater.* **66** 915–8
[17] Sim G-D, Lee Y-S, Lee S-B and Vlassak J J 2013 Effects of stretching and cycling on the fatigue behavior of polymer-supported Ag thin films *Mater. Sci. Eng.* A **575** 86–93
[18] Krawczyk K K, Groten J, Glushko O, Krivec M, Frühwirth M, Schulz G, Wolf C, Hartmann D, Moser M and Cordill M J 2021 Self-reducing silver ink on polyurethane elastomers for the manufacture of thin and highly stretchable electrical circuits *Chem. Mater.* **33** 2742–55
[19] Matsuhisa N, Inoue D, Zalar P, Jin H, Matsuba Y, Itoh A, Yokota T, Hashizume D and Someya T 2017 Printable elastic conductors by *in situ* formation of silver nanoparticles from silver flakes *Nat. Mater.* **16** 834–40
[20] Kim J and Kim W S 2014 Stretching silver: printed metallic nano inks in stretchable conductor applications *IEEE Nanotechnol. Mag.* **8** 6–13
[21] Borghetti M, Serpelloni M, Sardini E and Pandini S 2016 Mechanical behavior of strain sensors based on PEDOT: PSS and silver nanoparticles inks deposited on polymer substrate by inkjet printing *Sens. Actuators* A **243** 71–80
[22] Cahn G, Pierron O and Antoniou A 2021 Electrical performance evolution and fatigue mechanisms of silver-filled polymer ink under uniaxial cyclic stretch *Flex. Print. Electron.* **6** 035008
[23] Koshi T, Nomura K-I and Yoshida M 2021 Measurement and analysis on failure lifetime of serpentine interconnects for e-textiles under cyclic large deformation *Flex. Print. Electron.* **6** 025003
[24] Merilampi S, Laine-Ma T and Ruuskanen P 2009 The characterization of electrically conductive silver ink patterns on flexible substrates *Microelectron. Reliab.* **49** 782–90
[25] Mohammed A and Pecht M 2016 A stretchable and screen-printable conductive ink for stretchable electronics *Appl. Phys. Lett.* **109** 184101
[26] Sliz R, Huttunen O-H, Jansson E, Kemppainen J, Schroderus J, Kurkinen M and Fabritius T 2020 Reliability of R2R-printed, flexible electrodes for e-clothing applications *npj Flex. Electron.* **4** 1–9
[27] Suikkola J, Björninen T, Mosallaei M, Kankkunen T, Iso-Ketola P, Ukkonen L, Vanhala J and Mäntysalo M 2016 Screen-printing fabrication and characterization of stretchable electronics *Sci. Rep.* **6** 1–8
[28] Li Q, Antoniou A and Pierron O N 2022 Understanding resistance increase in composite inks under monotonic and cyclic stretching *Flex. Print. Electron.* **7** 045010
[29] Cahn G, Pierron O and Antoniou A 2021 Trace width effects on electrical performance of screen-printed silver inks on elastomeric substrates under uniaxial stretch *J. Appl. Phys.* **130** 115304
[30] Cahn G, Barrios A, Graham S, Meth J, Antoniou A and Pierron O 2020 The role of strain localization on the electrical behavior of flexible and stretchable screen printed silver inks on polymer substrates *Materialia* **10** 100642